Regenspurg *et al. Geotherm Energy (2017) 5:11*
DOI 10.1186/s40517-017-0069-9

Geothermal Energy

RESEARCH Open Access

Copper precipitation as consequence of steel corrosion in a flow-through experiment mimicking a geothermal production well

Simona Regenspurg[1*], Ives Geigenmüller[2], Harald Milsch[1] and Michael Kühn[3]

*Correspondence:
regens@gfz-potsdam.de
[1] Section 6.2 Geothermal Energy Systems, GFZ German Research Centre for Geosciences, International Centre for Geothermal Research (ICGR), Telegrafenberg, 14473 Potsdam, Germany
Full list of author information is available at the end of the article

Abstract

Decreasing production rates and massive precipitation of native copper (Cu(0)) were observed in the production well at the geothermal research facility Groß Schönebeck (Germany). The Cu precipitates filling up the well are a product of an electrochemical corrosion reaction between dissolved copper (Cu^{2+}, Cu^{+}) in the brine and iron (Fe(0)) of the carbon steel liner. It was hypothesized that this reaction occurs not only within the borehole, but also on the outside of the casing at contact between casing and reservoir rock as well as in the pores of the reservoir rock. To verify the assumption of potential clogging of the rock pores as well as to quantify the reaction and to determine reaction kinetics, a flow-through experiment was designed mimicking the reaction at depth of the well between sandstone samples (24 cm^3 Fontainebleau), steel (carbon steel or stainless steel), and artificial formation water containing 1 mM Cu^{2+} at oxic or anoxic (O_2 < 0.2 mg/L) conditions in dependence of temperature and salinity. Obtained experimental data served as input for a numerical reaction model to deepen the process understanding and that ultimately should be used to predict processes in the geothermal reservoir. Results showed that (1) with increasing temperature, the reaction rate of the electrochemical reaction increased. (2) High amounts of sodium and calcium chloride (NaCl + $CaCl_2$) in the solution decreased the overall reaction inasmuch more Fe and less Cu was measured in the salt-poor solutions over time. (3) Strongest oxidation was observed in oxic experiments when not only native copper but also iron hydroxides were identified after the experiments in the pore space of the rock samples. (4) No reaction products were observed when stainless steel was used instead of carbon steel to react with the Cu^{2+} solution. A numerical flow-through reactor model was developed for PHREEQC based on the assumption that Fe(0) corrosion is kinetically controlled and subsequent Cu(0) precipitation occurs in thermodynamic equilibrium within the investigated experimental set-up. Calculated coefficients of determination comparing measured and simulated reaction rates for Fe and Cu underline the validity of the approach.

Keywords: Saline fluids, Elevated temperature, Copper, Carbon steel, Flow-through experiments, Electrochemical reaction, Corrosion, PHREEQC modeling

Background

Mineral precipitation in the pores of geothermal reservoir rocks reduces the permeability and thus productivity and injectivity of geothermal wells (Putnis and Mauthe 2001; Milsch et al. 2009; Civan 2015). To prevent the threat of reservoir formation damage, the geochemical reactions within the pore space of the reservoir rock need to be understood and predictive models need to be developed. Precipitation is caused by shifts of the chemical equilibrium due to changes of the temperature, pressure, or interactions between geothermal fluid, reservoir rock, and the material of the well casing. However, processes in the reservoir rock can hardly be quantified or exactly predicted because access to the great depths of geothermal reservoirs is nearly impossible. Therefore, understanding, quantification, and determination of reaction kinetics are only possible by firstly mimicking of those processes on the laboratory scale. For simulating geothermal conditions, this approach requires an experimental set-up at elevated fluid temperatures, pressures, and salinity. The obtained experimental results represent a dataset that secondly can be used as basis for geochemical models to give prognoses about processes in the wells.

The purpose of the presented study is to test a hypothesis regarding the geothermal research facility Groß Schönebeck (North German Basin), where the well productivity had continuously decreased over time (Reinsch et al. 2015). It is assumed that clogging of reservoir rock pores in the near vicinity of the production well led to the reduced productivity (Regenspurg et al. 2015).

Briefly, the site can be described as follows: a well doublet has been drilled into a Permian sandstone and volcanic rock reservoir (Zimmermann et al. 2011). The reservoir fluid at around 4100 m depth is a Ca–Na–Cl brine with a temperature of about 150 °C that contains 265 g/L total dissolved solids (Regenspurg et al. 2010; Zimmermann et al. 2011). During circulation tests in 2011 and 2012 a strong decrease in reservoir productivity was observed over time (Blöcher et al. 2016). Simultaneously, it was detected that the production well was filled for around 200 m with material consisting predominantly of native copper (Cu(0); about 50%), together with magnetite (Fe_3O_4) and other minerals (Regenspurg et al. 2015). Based on these observations, it was assumed that Cu(0) forms as corrosion product by the electrochemical reaction of Cu^{2+}or Cu^{+}-containing fluid with Fe(0) of the carbon steel liner at depth (Regenspurg et al. 2015). It was further hypothesized that this reaction also occurs within the reservoir rock on the outer side of the steel casing, where Cu scales would clog the pores of the rock (Regenspurg et al. 2015), which could explain the observed reduction in production rates (Blöcher et al. 2016).

The assumption was tested and quantified in this study. A lab experiment was designed that reproduces the electrochemical reaction in dependence of temperature, salinity, and oxygen content. The experimentally obtained data (pH value, redox potential Eh, Fe, and Cu concentration) were implemented in a numerical flow-through reactor model that ultimately is supposed to be used to predict those redox reactions in the reservoir.

Methods

Experimental setup

The experiments simulate the flow of geothermal brine from the reservoir through the casing into the geothermal well. Capillaries of either RS carbon steel or 1.4307 stainless steel represent the casing and Fontainebleau quartz arenite samples (99.98% quartz)

with a permeability of ca. 100 × 10^{-15} m^2 (e.g. Haddad et al. 2006; Revil et al. 2014) represent the reservoir rock.

For each flow-through experiment, a new steel capillary (30 mm length; 6 mm outer diameter; 3 mm inner diameter) was inserted into the cylindrical rock samples (each 50 mm in length, 25 mm in diameter). Each assembly of rock and steel capillary was placed into a 5 L "reservoir container" yielding 1 mM $CuCl_2$ and a background of either deionized water or brine (deionized water with 2 M NaCl and 1.5 M $CaCl_2$; Fig. 1). The artificial geothermal fluids were pumped with a peristaltic pump through the steel capillary, which was connected via a tube to a "collecting container" (Fig. 1). The initial pumping rate was adjusted to 60 mL/h and re-adjusted due to decreasing flow rates over time within most experiments. Both containers were continuously mixed with magnetic stirrers and kept at constant temperature of 25, 50, or 80 °C.

One oxic experiment was performed at 25 °C with carbon steel and synthetic brine (experiment O, Table 1). For all other experiments, anoxic conditions were established by purging the solutions permanently with Argon (Ar). Dissolved oxygen was monitored at 25 and 50 °C by oxygen probes installed in the reservoir container. Monitoring

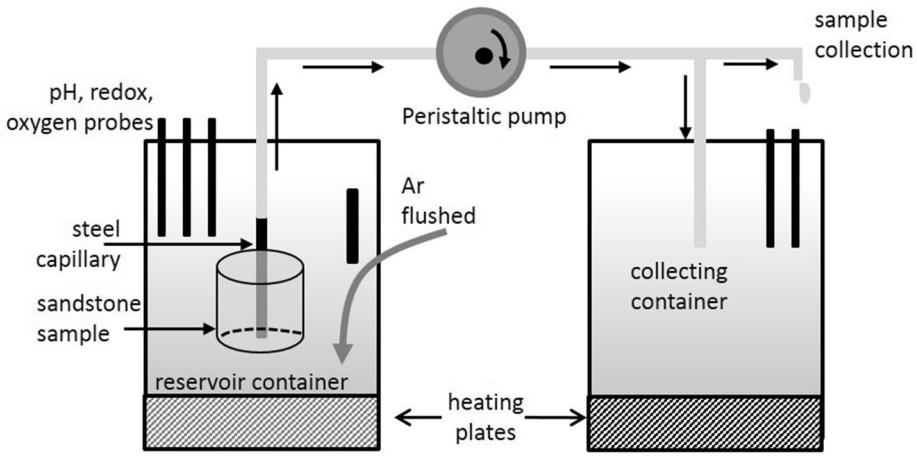

Fig. 1 Experimental set-up: Brine of different composition is pumped from the anoxic reservoir container via a peristaltic pump under anoxic conditions (Ar-purged) into the collecting container through a steel capillary that is inserted in a rock sample. After the reaction, the fluid can be sampled or collected in the collecting container (for experimental conditions see Table 1). Probes measuring pH, redox, and oxygen are installed in both containers. Temperatures can be adjusted by heating up the containers on a heating plate

Table 1 Composition and conditions of experimental solutions in the reservoir container. All solutions contain initially 1 mM Cu

Experiment name	Oxygen	Temperature (°C)	Salt content	Type of steel	Others
O	Oxic	25	2 M NaCl, 1.5 M $CaCl_2$	Carbon steel	
A	Anoxic	25	2 M NaCl, 1.5 M $CaCl_2$	Carbon steel	
B	Anoxic	50	2 M NaCl, 1.5 M $CaCl_2$	Carbon steel	
C	Anoxic	80	2 M NaCl, 1.5 M $CaCl_2$	Carbon steel	
D	Anoxic	80	0	Carbon steel	Perforated capillary
E	Anoxic	80	2 M NaCl, 1.5 M $CaCl_2$	Stainless steel	

of O_2 was not possible for the 80 °C experiments due to the low heat resistivity of the probe. However, the solutions were Ar-purged under the same conditions as during the experiments performed at lower temperature. Experiments A, B, and C were performed in duplicates with 2 M NaCl and 1.5 M $CaCl_2$ at 25, 50, or 80 °C, respectively. No Ca and Na salts were added in experiment D and the carbon steel capillary was perforated allowing an increased flow. Experiment E resembled experiment C but stainless steel was used instead of carbon steel (Table 1).

In all experiments, the pH value and redox potential were continuously monitored by probes in both containers (Fig. 1). After 0.1, 1, 1.5, 2, 3, 4, 6, 25, 27, 30, and 49 h (h), each 10 mL sample was taken directly from the fluid line (Fig. 1). The samples were immediately acidified to pH < 2 and analyzed for total Cu and Fe concentration.

Copper and iron measurement correction factors

Due to the impact of highly saline solutions on the measurement of metal concentration, correction factors were determined for Cu and Fe solutions in dependence of salinity. For this purpose, solutions of varying salinity (0.5, 1, 2, 4, 5 M NaCl) and either 1 mM Cu^{2+} (63.5 mg/L) or 1 mM Fe^{2+} (55.8 mg/L) were prepared. The Fe^{2+} solutions were prepared under anoxic conditions. After 24 h equilibration time, solutions were acidified, diluted (1:100), and measured in duplicates by inductive coupled plasma mass spectrometry (ICP-MS) with a Thermo Fisher Scientific Element XR instrument.

A strong dependency was found between increasing NaCl concentration and decreasing measured Cu concentration (Fig. 2, left). This allowed determining the instrument-specific correction factor for Cu measurements in 5 M chloride solution, which can be obtained from the slope (Fig. 2, right). All Cu^{2+} concentrations measured in 5 M chloride were corrected with this factor (0.61).

A similar test but with Fe^{2+} instead of Cu^{2+} indicated that a correction for this metal is not required, because the measured Fe concentration equaled the Fe^{2+} concentration added to the samples at chloride concentration between 0 and 5 M.

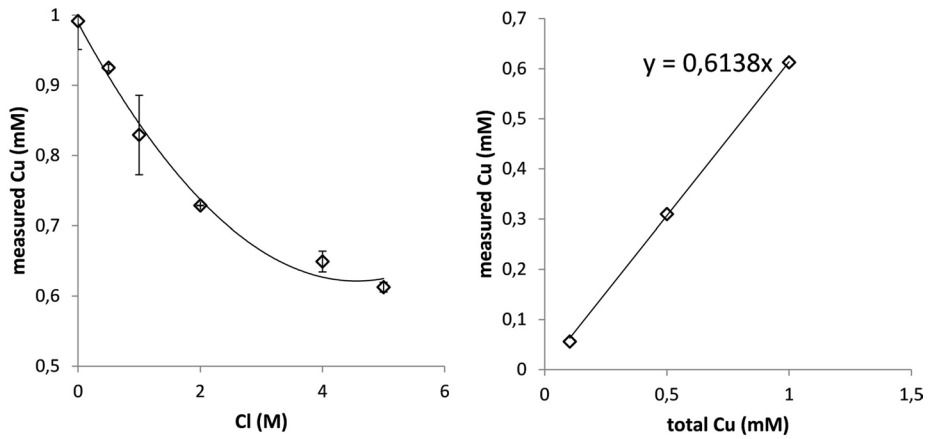

Fig. 2 *Left* measured Cu concentration after addition of 1 mM Cu into solution containing 0, 0.5, 1, 2, 4, and 5 M NaCl. *Right* comparison of measured with total (real) Cu concentration in 5 M chloride solution

Solid phase analysis

Before and after each experiment, both the rock samples and the capillaries were dried at 105 °C and kept in a desiccator. After the experiments, the capillaries were separated from the rock and rock samples were transected perpendicular to the capillary. Polished thin sections of these cuts were prepared, embedded into epoxy resin, and analyzed after Ag_2O vaporization by electron microprobe (EMP; JEOL JXA-8530F Hyperprobe). One rock sample (experiment C) was analyzed before thin section preparation by X-ray computer tomography (CT) to obtain 2D and 3D recordings of the pore space microstructure by a GE phoenixIx-ray nanotom 180 NF µCT equipped with a 180 kV/15 W X-ray tube and a 5 Mpixel detector. The recordings were obtained in <1° steps during one 360° rotation and assembled to a 3D picture with a resolution of 30 µm by numerical reconstruction (Goebel et al. 2012). After thin section preparation, all rock samples were cut parallel to the capillary direction along the perpendicular axis for visual analysis of pore space clogging.

Modeling approach

For the development of any mathematical or physical model a general approach needs to be followed even though specific differences exist between analytical, conceptual, or data driven models (Araghinejad 2014). At first, the purpose of the required model needs to be defined. Second, the model needs to be conceptualized. Third, the methods are selected and fourth the model is calibrated or trained with a subset of the available data to enable quantification in the first place. In the last step, before the developed model can be applied for predictive purposes, it needs to be evaluated with an independent subset of the data at hand.

The purpose of the model presented here is to quantify the experimental observations of the electrochemical reactions observed during the laboratory experiments. The numerical experiment of the presented study was conceptualized assuming the sandstone sample together with the capillary to be a zero-dimensional flow-through reactor. Inflow and outflow of the artificial geothermal formation water were deduced from the pore volume of the rock sample, the size of the capillary, and the pumping rate of 60–100 mL/h during the experiments. The residence time of the solution containing 1 mM Cu^{2+} within the experimental set-up of rock sample and capillary was 0.6–1.5 min. The time step was fixed to 1 min. For each step 2.5 mL solution was added to and removed from the reactor.

Method selection is based on the hypothesis that the applied rate equation for each time step during the reaction is based on the fact that Fe(0) in contact with formation water is thermodynamically unstable and therefore oxidizes (Schüring et al. 2000). The primary iron phase dissolves. The released electrons are transferred to the Cu^{2+} ions that are in contact with the steel capillary. They reduce Cu^{2+} ions to Cu(0) that precipitates both, inside the capillary and outside within the sandstone sample. It was further assumed that the corrosion rate of Fe(0) governs the redox reaction kinetically. Copper, on the other hand, as secondary phase, precipitates whenever supersaturated under the assumption that the reduction reaction is thermodynamically regulated.

For the numerical simulations with the software PHREEQC (version 3.3.5-10806; Parkhurst and Appelo 1999) the database "phreeqc.dat" was extended with the redox reactions of iron (Eq. 1) and copper metal (Eq. 2).

$$\mathrm{Fe} = \mathrm{Fe}^{2+} + 2\mathrm{e}^{-} \quad (\log K - 12.55) \tag{1}$$

$$\mathrm{Cu} = \mathrm{Cu}^{2+} + 2\mathrm{e}^{-} \quad (\log K - 9.705) \tag{2}$$

The reaction rate equation (Eq. 3) is defined with a rate constant k. A second term limits the reaction progress of the Fe(0) corrosion with the saturation state of amorphous iron hydroxide ($SR_{Fe(OH)3(a)}$). Kühn et al. (1998) showed for geothermal brines that this is the phase best to quantify measured redox potentials and Fe content. The third term in the equation is the ratio between the total amount of Cu^{2+} increasing during the reaction and the amount of precipitated Cu(0) per time step and its increasing reactive surface area, which increases the reaction rate. The additional factor 7 adjusts the slope of the reaction rate. Cu(tot) is the total amount of copper precipitated and Cu(p) the amount of Cu precipitated during a time step:

$$\mathrm{rate} = k * \left(1 - \mathrm{SR}_{(\mathrm{Fe(OH)3a})}\right) * \mathrm{Log}\left(10 + \frac{\mathrm{Cu(tot)}}{\mathrm{Cu(p)}} * 7\right) \tag{3}$$

All input data (the solution composition, temperature, pH, redox, amount of Fe, and the time parameters) were taken or derived from the laboratory experiments. Charge balance at the beginning of the simulations was acquired via the chloride ions. The simulation procedure proceeded after the model design (Eq. 3) with the calibration of the system based on the salt-free experiment (Table 1, experiment D). After this has been done, the derived model was applied to the experiments with the saline solution (Table 1, experiment C).

Even though the Debye–Hückel theory for calculating ion activities in solution is inaccurate for highly saline brines, there was no choice because the Pitzer formalism applicable for those brines is not available for redox reactions (Kühn 2009). However, it was shown before that the ferrous and ferric system can be accurately described based on Debye–Hückel even in geothermal brines (Kühn et al. 1998). To be more confident with the modeling results, the calibration step was performed based on the salt-free experiment for which the ion activity calculations using the Debye–Hückel approach are perfectly valid. Afterwards, the unchanged model was applied to the experiment with the saline solution for independent evaluation.

Results

Experimental solutions

The measured initial pH values of the artificial brine in the reservoir container were between 4.8 and 4.6 and the redox potentials between 530 and 460 mV. In the oxic experiment, the pH decreased to 3.3 and the redox potential to 290 mV. In all other experiments, anoxic conditions were confirmed by dissolved oxygen measurements (O_2 < 0.2 mg/L). The pH values measured of the anoxic experiments within the collection container (cumulative fluid) after reaction with the sample (rock plus capillary) decreased to 3.9 (at 25 °C), 3.0 (at 50 °C), and 2.8 (at 80 °C; Fig. 3a). Similarly, redox

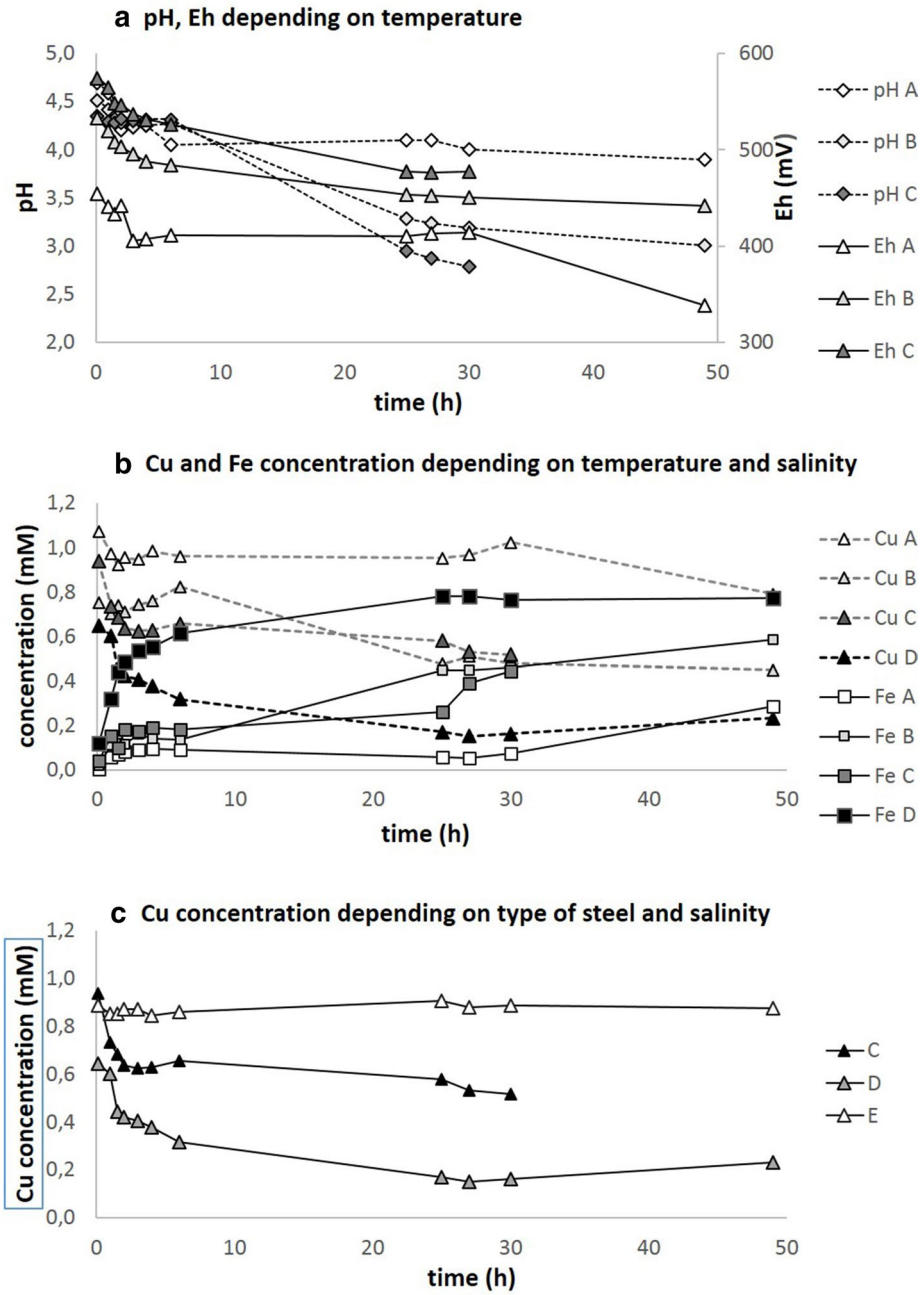

Fig. 3 Measured solution parameters in experiments *A*–*E*. **a** Eh and pH values at 25 (*A*), 50 (*B*), and 80 (*C*) °C in the collection container. **b** Cu and Fe concentrations measured over time in samples from the sampling line. **c** Cu concentration at 80 °C experiments in brine collected from the sampling line (*C*); in deionized water (*D*); in brine with stainless steel capillary (*E*). Details on experiments *A*, *B*, *C*, *D*, *E* are explained in Table 1

values, of the anoxic experiments decreased to 338 mV (at 25 °C), 442 mV (at 50 °C), and 477 mV (at 80 °C), respectively (Fig. 3a). Iron and Cu concentrations were measured in samples taken directly from the fluid line after reaction with the sample (rock plus capillary). They are more precise as compared to pH and redox measurements that were measured in the accumulated fluid in the collection container (Fig. 1). Decreasing

concentration of Cu and an increasing amount of Fe was determined over time in all experiments apart of those performed with stainless steel (Fig. 3 b, c). This reaction was increased with increasing temperature (Fig. 3b).

Using stainless steel instead of carbon steel significantly inhibited the reaction as observed by both, low and constant Fe concentrations (0.01–0.04 mM) and high and constant Cu concentrations (0.9 mM; Fig. 3c). However, stainless steel experiments also showed a decrease of the pH value from 4.9 to 4.1 and of the redox potential from 550 to 487 mV.

Solid phase analysis

Visually, the rock samples differed strongly after the oxic experiment O, as compared to the anoxic treated samples (Fig. 4). This is obvious by the large (4 mm), red reaction area around the capillary (Fig. 4) significant of the oxic experiment. In contrast, the anoxic treated samples without brine addition (D) showed a very narrow (1 mm), dark-brownish reaction seam, and the anoxic experiments with brine addition resulted in a large reaction seam (through the entire sample) with orange–brown colors close to the capillary and bluish color at greater distance (Fig. 4).

Thin sections prepared from all rock samples after each experiment were analyzed with an electron microprobe. Grey shades in the picture indicate the density of the material (Fig. 5): black areas correspond to pore space, whereas white areas indicate material of highest density. EDX measurements at selected locations could semi-quantitatively identify the sandstone matrix of grey quartz grains (examples in Fig. 5). The pore space was partially filled with material containing Ca, Fe, and Cu (Fig. 5; all elemental

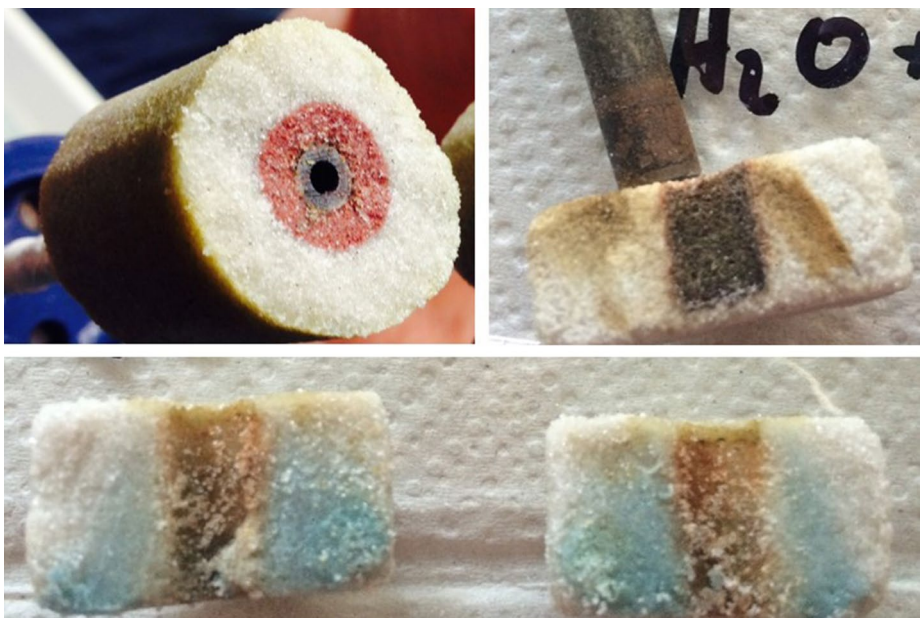

Fig. 4 Rock samples cut open after the reaction of carbon steel with synthetic Cu-containing fluid: *Top left* oxic experiment (O) opened immediately after removal from the brine. *Top right* anoxic experiment D with no additional chloride salt; Bottom experiment C: anoxic with brine. Pictures of experiment C and D were taken some weeks after the experiments

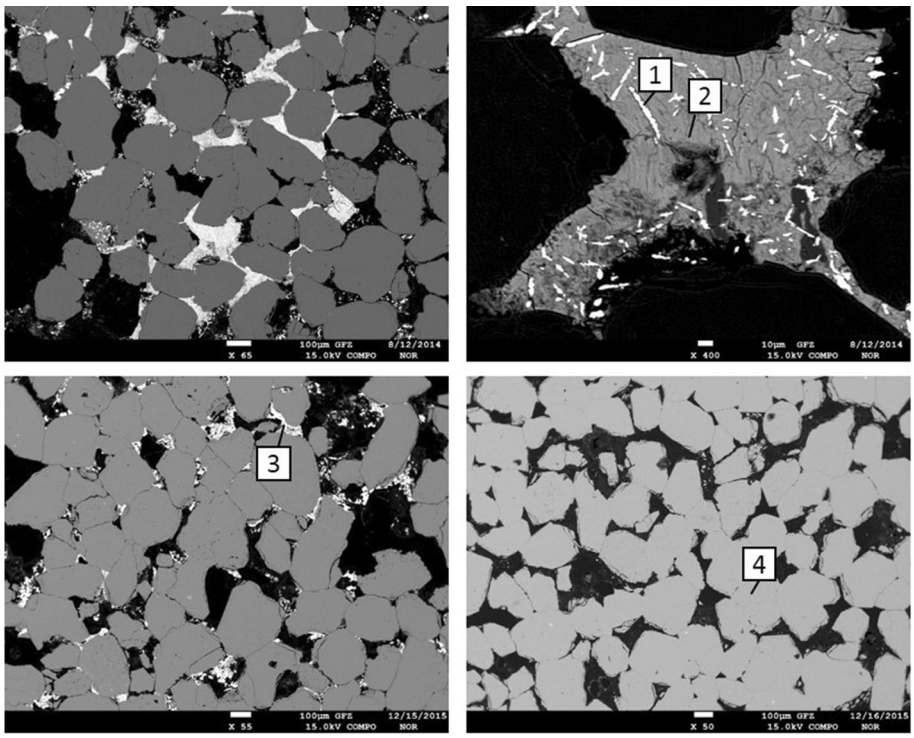

	CuO	FeO	CaO	SiO_2	Cl
1	91.8	6.5	1.8	0	0
2	0	86.2	13.8	0	0
3	76	0	14	0	10.4
4	0	0	0	100	0

EDX results (%) at locations indicated by black lines

Fig. 5 Electron microprobe pictures of rock thin sections after the experiments: *Roundish grey areas* represent quartz particles of the sandstone; *black areas* indicate pore space; *white areas* indicate high-density. *Top left* oxic-treated sandstone sample (O). *Top right* enlargement of one pore of the *top–left* picture filled with Fe-hydroxides (*grey areas*) and pure Cu (*white needle-shaped areas*). *Bottom left* sample from experiment C; *Bottom right* sample from experiment E (use of stainless steel) with intact pore space. The corresponding table shows semi-quantitative EDX results of elemental composition of four different locations as indicated by *numbers*

concentrations were given as oxides). In thin sections of the oxic-treated experiment, pores are filled not only with white precipitates consisting of Cu(0) but also with light grey areas of iron oxide (Fig. 5, top right). The thin section of experiment E did not show the formation of any precipitate in the pores (Fig. 5, bottom right).

Computer tomographic measurements were performed of the rock sample after the anoxic experiment C (brine + 80 °C). The resulting 3D picture shows areas with elevated densities that are predominantly located at the bottom (capillary inflow) and along the outer capillary wall (in white; Fig. 6).

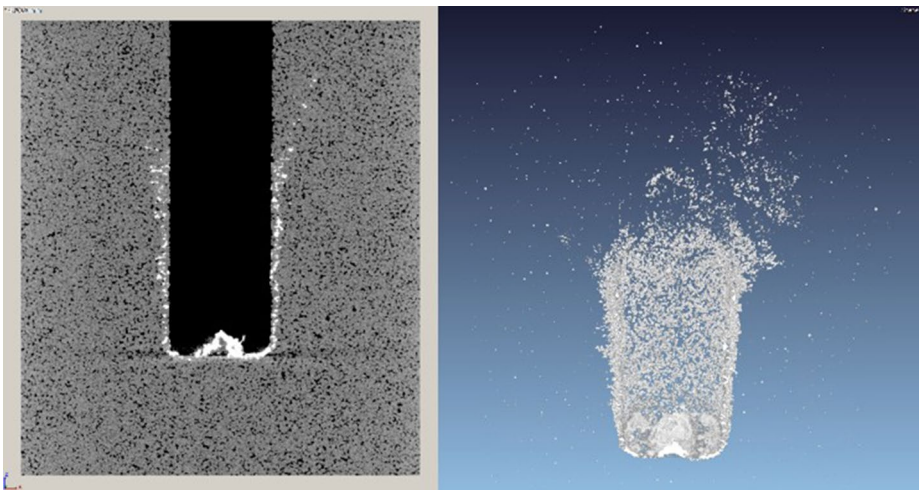

Fig. 6 Computer tomographic (CT) images of one rock sample after the flow-through experiment (Experiment C; 80 °C). *White areas* indicate precipitation of a high-density material in the pores of the rock. *Left* 2D, *right* 3D image

Numerical simulations

The numerical simulations reach steady-state concentrations of Fe and Cu in the outflow of the experiments within 10–20 h (Fig. 7). For the salt-free solution, the process stabilizes a little bit faster as compared to the experiment with the salt-rich brine solution. In the same way, on the one hand, the progress of the reaction reaches a higher reduction of Cu(0) of up to 0.3 mM and higher increase of Fe of up to 0.7 mM for the salt-free experiment (Fig. 7, Experiment D). On the other hand, within the salt-rich brine the resulting Cu concentration is 0.5 mM and the Fe concentration is 0.3 mM (Fig. 7, Experiment C).

PHREEQC calculations were performed based on the Debye–Hückel theory for calculation of ion activities to allow simulation of redox reactions. Therefore, the salt-free Experiment D was used to fit the described rate equation, which was then used in the exact same way for Experiment C with the salt-rich solution. Within Experiment D the measured concentration of Cu is simulated with a coefficient of determination (r^2) of 0.69 and for Fe with 0.83, which can be considered as a fairly good result. A value for r^2 of 0.5 is seen as minimum for an acceptable representation of measured data by the

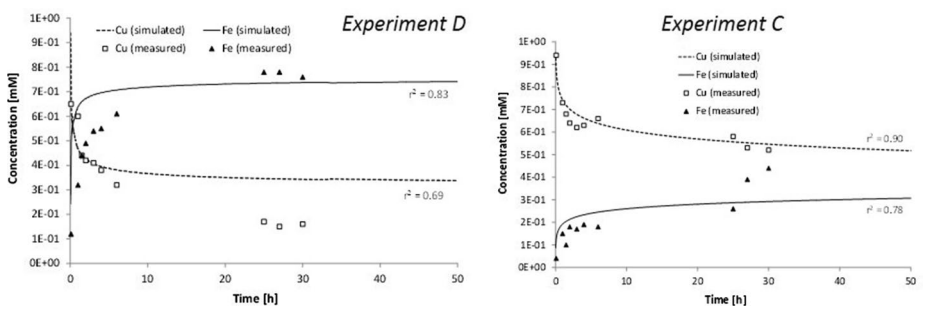

Fig. 7 Simulated data compared to experimental measurements of Cu and Fe concentration as result of the redox reaction. *Left* Experiment D (anoxic, 80 °C, salt-poor); *Right* experiment C (anoxic, 80 °C, salt-rich brine)

applied numerical model (Moriasi et al. 2007). For Experiment C, within the evaluation step, the simulation results represent the measured Cu concentrations even better with an r^2 of 0.90 and a comparable accuracy of 0.78 for Fe.

Discussion

Rock flow-through experiments are well suited to determine the reactions between a fluid and a porous rock sample and to determine the reaction kinetics (e.g. Bourbie and Zinszner 1985; Knauss and Wolery 1988; Moghadassi et al. 2005). In this study, additionally the interaction with steel as a third reactive component was investigated. Steel plays a major role in geothermal reservoirs due to its use as casing and the high reactivity of Fe(0) in the subsurface at contact with water (Pound et al. 1985; Labjar et al. 2010). However, for investigation of reactions at geothermal conditions, either water–rock interaction (e.g. Savage et al. 1992) or steel corrosion is considered in literature (e.g. Pound et al. 1985; Mundhenk et al. 2013; Klapper et al. 2012; Bäßler et al. 2009).

In all flow-through experiments of this study conducted with carbon steel capillaries decreasing Cu and increasing Fe concentrations were measured (Fig. 3). This was expected since the electrochemical potential of carbon steel is much lower (−0.41 to −0.55 V) as compared to copper (−0.32 to −0.4 V; data determined for seawater; Steel Atlas 2010). Simultaneously, with decreasing Cu concentrations, precipitates had formed in the pores of the sandstone samples (Figs. 4, 5 and 6). In addition, due to the reducing flow rates during all experiments but experiment D (use of stainless steel), the peristaltic pump needed re-adjustment to ensure the continuity of the reaction. In experiment C, the flow rate decreased even to complete cessation of the pump after 30 h indicating clogging of the pore space (Fig. 3a, c).

Apart from the type of steel, the presence of oxygen plays the second most important role for steel corrosion and subsequent pore clogging: While in the presence of oxygen, several solid phases were identified to form in the pores of the rock (Fe-hydroxides and Cu(0)), in anoxic experiments only Cu(0) was detected (Fig. 5).

Effect of temperature

Increasing corrosion with increasing temperature is a well-known effect that can be explained by generally the higher reactivity of the components at elevated temperatures (e.g. Zarrouk et al. 2010). Experiments A, B, and C were conducted with solutions of the same chemical compositions with only the temperature varied (from 25 to 80 °C). In these experiments, the reaction seems enhanced with increasing temperature as obvious by decreasing pH and increasing redox potentials (Eh, Fig. 3). The decrease of the pH down to 2.5 (Fig. 8) is probably due to the formation of hydroxides (Cu or Fe) that remove OH^- from the solution and increase acidity. The increase of redox, on the other hand, is due to the formation of native Cu(0) that accepts the electrons from the corrosion and dissolution process of iron ($Cu^{2+} + 2e^- \rightarrow Cu(0)$) thus shifting the redox potential to more positive values. This effect of temperature dependent changes in chemistry is less obvious for measured Cu and Fe concentrations inasmuch the reaction peak (highest Fe and lowest Cu concentration) were measured already at a moderate temperature of 50 °C (Fig. 8). However, large error bars for Fe concentrations indicate potential precipitation/dissolution of solid Fe^{3+} phases. It needs also to be considered

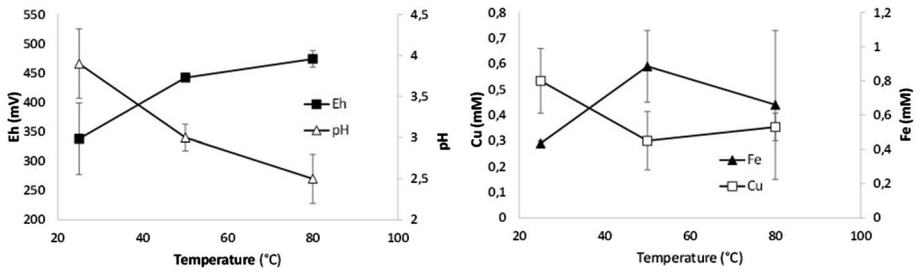

Fig. 8 Experimental data (A, B, C): effect of temperature on pH, Eh (*left*) as well as on Cu- and Fe concentration (*right*)

that sampling for pH and Eh measurements occurred in the collection container of an accumulated fluid, whereas Cu and Fe concentrations were measured from separated samples (punctual measurements). Possibly, at increased temperature a higher mobilization of Fe results in increased precipitation of iron oxide/hydroxide, which in turn results either in the adsorption and thus removal of Cu^{2+} from solution or in the formation of crystal seeds for Cu-hydroxide formation.

Effect of brine salinity

In all experiments but one (experiment D), a 5 M chloride solution was used as background electrolyte to mimic the salinity of brine that was determined at the geothermal reservoir Groß Schönebeck (Regenspurg et al. 2010). The high chloride contents in the fluid explain the good solubility of Cu due to the formation of aqueous Cu–Cl complexes (e.g. Doner 1978; Wells 1984; Regenspurg et al. 2015). Apparently, the presence of chloride slows down the precipitation reaction and the overall amount of Cu removed from solution in the salt-rich brine, because Fe(0) corrosion is inhibited in the first place with a decreased amount of Fe brought into solution, which is obvious both from the experimental and modeled data (Fig. 7). It can be assumed that the formation of aqueous Cu–Cl and Fe–Cl complexes reduces their ion activities and thus partially prevents the oxidation of Fe(0) to Fe^{2+} and with it the reduction of Cu^{2+} and its precipitation as Cu(0). Similarly, it was shown by equilibrium speciation calculations with PHREEQC (input pH of 5, as well as 5 M NaCl and 1 mM Cu), the most dominant Cu complex is uncharged $CuCl_2$, followed by $CuCl^+$, and Cu^{2+} species. While at 25 °C all solid Cu-phases are undersaturated, at 50 and 80 °C, the mineral atacamite ($Cu_4Cl_2(OH)_6$) is supersaturated with a saturation index of 0.6 and 2.35, respectively. The precipitation of a Cu-hydroxide phase would also confirm the observed decreasing pH values as well as the increased Cu concentration with increasing temperature from 50 to 80 °C (Fig. 8).

Comparison of experimental versus modeling results

Quantification of ion activities represents the base for all thermodynamically and kinetical reaction calculations. The ideal model for calculating activity coefficients should be highly consistent, of compact mathematical form, and of high accuracy over wide ranges of temperature, pressure, and concentration. However, none of the currently existing models satisfy all of these requirements (Kühn 2004; Zhu and Anderson 2002).

Therefore, especially simplified models have to be applied due to limited data sets (Kühn 2009; Walter et al. 1994). The simplification within the presented study is the approach to quantify the development of the iron and copper concentrations in solution of the laboratory experiments just by a kinetically controlled corrosion and dissolution reaction of iron and a thermodynamically governed precipitation of copper as secondary phase.

The two experiments simulated (C and D, Table 1; Fig. 7) differ only with respect to the amount of salt added as background electrolyte to the solutions. The more simplified way of ion activity calculations for dilute solutions was used to fit the reaction rate equation with the salt-free experiment based on kinetically governed corrosion of Fe from the steel capillary with subsequent Cu(0) precipitation from the solution in thermodynamic equilibrium. It can be applied for the salt-rich experiment right away with even slightly better results (Fig. 7). The simulation results for both experiments are within an acceptable range of accuracy shown by a coefficient of determination clearly above 0.5 (Moriasi et al. 2007).

High background salt concentrations reduce the reactive concentration (=activity) of Cu as well as Fe concentration in solution. As a result, the steady-state concentrations of both metals are significantly lower within the salt-rich experiment C compared to the salt-free Experiment D (Fig. 7). Further, a reduced activity in salt-rich solutions slows down the reaction rate as well. Steady-state is reached faster within the salt-free experiment D.

The coincidence between measured and simulated Cu and Fe concentrations confirm the assumption that Fe(0) corrosion is kinetically controlled and subsequent Cu(0) precipitation occurs in thermodynamic equilibrium. This is a good way to quantify the reaction rates of potential electrochemical reactions within geothermal production wells.

Conclusions

The performed experiments mimic field observations from the geothermal research site Groß Schönebeck, where fluid–casing–rock interactions were assumed to be responsible for clogging the pores of the reservoir rock near the production well casing. To find evidence for this hypothesis, simplified experiments were conducted and the effects of oxygen, salinity, temperature, and type of steel on the reactions were determined. The type of steel was found to have the largest effect on the electrochemical corrosion at geothermal conditions. If the type of steel is nobler as compared to copper, the electrochemical reaction is prevented. However, in geothermal wells, the material of choice for application as casing material is carbon steel and therefore a reaction with Cu can be expected if the fluid contains dissolved Cu. The effect of dissolved oxygen in solution is also rather large. However, since in a natural deep geothermal system, hardly any dissolved oxygen occurs, this parameter is of more relevance in either more shallow reservoirs or when air is pumped into a geothermal well for example during a lift-test. Usually, temperature, pressure, and salinity at depth are the factors that predominantly control the investigated electrochemical reaction. It was shown that due to chloride complex formation of Cu and Fe, electrochemical reaction rates are lower in highly saline solutions. The effect of temperature differs depending of the type of saturated/precipitating Cu mineral.

Based on the experimental dataset provided here, a numerical flow-through reactor model for quantification of electrochemical reactions at elevated temperatures and salinities was developed and reaction rates and the progress of reaction with numerical simulations were quantified. Within the model Fe(0) oxidation is kinetically controlled and subsequent copper precipitation occurs in thermodynamic equilibrium. Calculated coefficients of determination confirm the approach to quantify the investigated redox reaction rates.

In the next step, this model can be used to predict the temporal and spatial extend at the field scale if implemented in 3D and finally will give clear indication of the relevance of the investigated electrochemical reaction.

Authors' contributions

SR main idea, supervision, data interpretation, corresponding author. IG experimental data collection as part of his Master Thesis. HM experimental design and scientific discussion. MK geochemical modeling. All authors read and approved the final manuscript.

Author details

[1] Section 6.2 Geothermal Energy Systems, GFZ German Research Centre for Geosciences, International Centre for Geothermal Research (ICGR), Telegrafenberg, 14473 Potsdam, Germany. [2] Applied Geosciences, Technical University of Berlin, Berlin, Germany. [3] 3.4 Fuid Systems Modelling, GFZ German Research Centre for Geosciences, Telegrafenberg, 14473 Potsdam, Germany.

Acknowledgements

We kindly acknowledge Felix Bosien and Tanja Ballerstedt for great technical support, Oona Appelt for electron EMP- and Iris Pieper for ICP-OES (TU Berlin) and Heike Rothe for ICP-MS measurements. We also want to thank Erik Rybacki for computer tomographic measurements.

Competing interests

The authors declare that they have no competing interests.

Availability of data and materials

All datasets on which the conclusions of the manuscript rely to are presented in the main paper.

Funding

Funding was provided from Helmholtz Centre Potsdam, GFZ German Research Centre for Geosciences.

Publisher's Note

Received: 27 March 2017 Accepted: 30 June 2017
Published online: 06 July 2017

References

Araghinejad S. Data-driven modeling: using MATLAB® in water resources and environmental engineering. Dordrecht: Springer Science+Business Media; 2014.

Bäßler R, Burkert A, Saadat A, Kirchheiner R and Finke M. Evaluation of corrosion resistance of materials for geothermal applications. In: Corrosion. NACE International: Houston; 2009.

Blöcher G, Reinsch T, Henninges J, Milsch H, Regenspurg S, Kummerow J, Francke H, Kranz S, Saadat A, Zimmermann G, Huenges E. Hydraulic history and current state of the deep geothermal reservoir Groß Schönebeck. Geothermics. 2016;63:27–43.

Bourbie T, Zinszner B. Hydraulic and acoustic properties as a function of porosity in Fontainebleau sandstone. J Geophys Res Solid Earth. 1985;90(B13):11524–32.

Civan F. Reservoir formation damage. Houston: Gulf Professional Publishing; 2015.

Doner HE. Chloride as a factor in mobilities of Ni (II), Cu (II), and Cd (II) in soil. Soil Sci Soc Am J. 1978;42(6):882–5.

Goebel THW, Becker TW, Schorlemmer D, Stanchits S, Sammis C, Rybacki E, Dresen G. Identifying fault heterogeneity through mapping spatial anomalies in acoustic emission statistics. J Geophys Res. 2012;117:B03310.

Haddad S, Worden R, Prior D, Smalley C. Quartz cement in the Fontainebleau sandstone, Paris Basin, France: crystallography and implications for mechanisms of cement growth. J Sed Res. 2006;76:244–56.

Kühn M. Modelling feedback of chemical reactions on flow fields in hydrothermal systems. Surv Geophys. 2009;30(3):233–51. doi:10.1007/s10712-009-9055-5.

Kühn M. Reactive flow modeling of hydrothermal systems. Lecture notes in earth sciences 103. Berlin: Springer; 2004.

Kühn M, Vernoux J-F, Kellner T, Isenbeck-Schröter M, Schulz HD. Onsite experimental simulation of brine injection into a clastic reservoir as applied to geothermal exploitation in Germany. Appl Geochem. 1998;13(4):477–90. doi:10.1016/S0883-2927(97)00081-4.
Klapper HS, Bäßler R, Weidauer K, Stürzbecher D. Evaluation of suitability of high-alloyed materials for geothermal applications in the North German basin. Corrosion. J Sci Eng. 2012;68(1):016001.
Knauss KG, Wolery TJ. The dissolution kinetics of quartz as a function of pH and time at 70 C. Geochim Cosmochim Acta. 1988;52(1):43–53.
Labjar N, Lebrini M, Bentiss F, Chihib NE, El Hajjaji S, Jama C. Corrosion inhibition of carbon steel and antibacterial properties of aminotris-(methylenephosphonic) acid. Mater Chem Phys. 2010;119(1):330–6.
Milsch H, Seibt A, Spangenberg E. Long-term petrophysical investigations on geothermal reservoir rocks at simulated in situ conditions. Transp Porous Media. 2009;77(1):59–78.
Moghadasi J, Müller-Steinhagen H, Jamialahmadi M, Sharif A. Model study on the kinetics of oil field formation damage due to salt precipitation from injection. J Petrol Sci Eng. 2004;43(3):201–17.
Moriasi D, Arnold J, Van Liew M, Bingner R, Harmel R, Veith T. Model evaluation guidelines for systematic quantification of accuracy in watershed simulations. Asaba: American Society of Agricultural and Biological Engineers ASABE; 2007.
Mundhenk N, Huttenloch P, Sanjuan B, Kohl T, Steger H, Zorn R. Corrosion and scaling as interrelated phenomena in an operating geothermal power plant. Corros Sci. 2013;70:17–28.
Parkhurst DL and Appelo CAJ. User's guide to PHREEQC (Version 2)—a computer software for speciation, batch-reaction, one-dimensional transport, and inverse geochemical calculations: US Geol Surv Water-Resour Investig Rep. 1999;99–4259.
Pound BG, Abdurrahman MH, Glucina MP, Wright GA, Sharp RM. The corrosion of carbon steel and stainless steel in simulated geothermal media. Aust J Chem. 1985;38(8):1133–40.
Putnis A, Mauthe G. The effect of pore size on cementation in porous rocks. Geofluids. 2001;1(1):37–41.
Regenspurg S, Wiersberg T, Brandt W, Huenges E, Saadat A, Schmidt K, Zimmermann G. Geochemical properties of saline geothermal fluids from the in situ geothermal laboratory Groß Schönebeck (Germany). –. Chemie der Erde–Geochem. 2010;70(3):3–12.
Regenspurg S, Feldbusch E, Byrne J, Deon F, Driba LD, Henninges J, Kappler A, Naumann R, Reinsch T, Schubert C. Mineral precipitation during production of geothermal fluid from a Permian Rotliegend reservoir. Geothermics. 2015;54:122–35.
Reinsch T, Regenspurg S, Feldbusch E, Saadat A, Huenges E, Erbas K, Zimmermann G, Henninges J. Reverse cleanout in a geothermal well: analysis of a failed coiled-tubing operation. SPE Prod Oper. 2015;30(04):312–20.
Revil A, Kessouri P, Torres-Verdin C. Electrical conductivity, induced polarization, and permeability of the Fontainebleau sandstone. Geophysics. 2014;79(5):301–18.
Savage D, Bateman K, Richards HG. Granite-water interactions in a flow-through experimental system with applications to the Hot Dry Rock geothermal system at Rosemanowes, Cornwall, UK. Appl Geochem. 1992;7(3):223–41.
Schüring J, Schulz HD, Fischer WR. Redox-fundamentals, processes and applications. Berlin: Springer; 2000. ISBN 978-3-540-66528-1.
Steel Atlas. ATLAS TECH NOTE No. 7 Galvanic corrosion; 2010. http://www.atlassteels.com.au.
Walter AL, Frind EO, Blower DW, Ptacek CJ, Molson JW. Modeling of multicomponent reactive transport in groundwater. 1. Model development and evaluation. Water Resour Res. 1994;30:3137–48.
Wells AF. Structural inorganic chemistry. 5th ed. Oxford: Oxford University Press; 1984.
Zarrouk A, Warad I, Hammouti B, Dafali A, Al-Deyab SS, Benchat N. The effect of temperature on the corrosion of Cu/HNO3 in the presence of organic inhibitor: part-2. Int J Electrochem Sci. 2010;5(10):1516–26.
Zhu C, Anderson G. Environmental applications of geochemical modeling. Cambridge: Cambridge University Press; 2002.
Zimmermann G, Blöcher G, Reinicke A, Brandt W. Rock specific hydraulic fracturing and matrix acidizing to enhance a geothermal system–concepts and field results. Tectonophysics. 2011;503(1–2):146–54.